

Nanoscale Viscosity of Cytoplasm Is Conserved in Human Cell Lines

Karina Kwapiszewska,* Krzysztof Szczepański, Tomasz Kalwarczyk, Bernadeta Michalska, Paulina Patalas-Krawczyk, Jędrzej Szymański, Tomasz Andryszewski, Michalina Iwan, Jerzy Duszyński, and Robert Holyst*

Cite This: *J. Phys. Chem. Lett.* 2020, 11, 6914–6920

Read Online

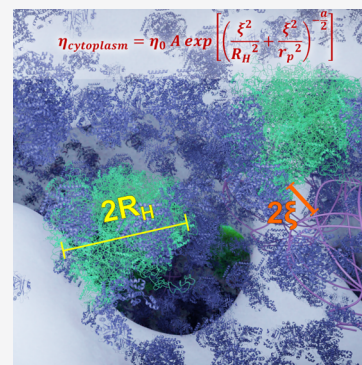
ACCESS |

Metrics & More

Article Recommendations

Supporting Information

ABSTRACT: Metabolic reactions in living cells are limited by diffusion of reagents in the cytoplasm. Any attempt to quantify the kinetics of biochemical reactions in the cytosol should be preceded by careful measurements of the physical properties of the cellular interior. The cytoplasm is a complex, crowded fluid characterized by effective viscosity dependent on its structure at a nanoscopic length scale. In this work, we present and validate the model describing the cytoplasmic nanoviscosity, based on measurements in seven human cell lines, for nanoprobe ranging in diameters from 1 to 150 nm. Irrespective of cell line origin (epithelial–mesenchymal, cancerous–noncancerous, male–female, young–adult), we obtained a similar dependence of the viscosity on the size of the nanoprobe, with characteristic length-scales of 20 ± 11 nm (hydrodynamic radii of major crowders in the cytoplasm) and 4.6 ± 0.7 nm (radii of intercrowder gaps). Moreover, we revealed that the cytoplasm behaves as a liquid for length scales smaller than 100 nm and as a physical gel for larger length scales.



Metabolism at the cellular level is considered as a network of reactions between biomolecules.^{1,2} These reactions maintain a balance where any prolonged disturbance can lead to pathological changes, including cell death or systemic diseases.^{3,4} From the physical point of view, a reaction can occur when molecules of reagents approach each other. In an equilibrium-state solution, Brownian motion (free diffusion) is a source of the movement of particles, and an increase of diffusion rate increases the probability of molecular encounters leading to biochemical reactions. The cytoplasm is a complex and crowded medium, where diffusion of biomolecules is hindered, and therefore diffusion can be treated as a factor limiting reaction rates in a cell.^{5,6} Decrease of diffusion rates would decrease rates of metabolic reactions and could lead to cell damage.⁷

According to the Stokes–Einstein–Einstein relation,^{8,9} the diffusion coefficient depends inversely on hydrodynamic drag, $f = 6\pi\eta_{\text{eff}}r_p$, where r_p is the hydrodynamic radius of a probe and η_{eff} is an effective viscosity of the medium. Many reports show that viscosity of the cytoplasm is not constant, but rather spatially heterogeneous.^{10–12} Additionally, according to our research, scale-dependent heterogeneity of cytoplasmic viscosity is even more pronounced.^{13–15} We found that objects of different sizes can experience different viscosity: the viscosity increases with the increasing size of the object.¹³ It is an outcome of the complex composition of cytoplasm—various components provide obstacles at different length-scales: the only obstacle of similar or smaller size can hinder the diffusion of a probe (see Figure 1: I). Our previous, detailed works on polymer and colloidal solutions resulted in a comprehensive model of length-scale dependent viscosity (LSDV), applicable for complex fluids^{13,16–19}

$$\eta_{\text{eff}} = \eta_0 A \exp \left[\left(\frac{\xi^2}{R_H^2} + \frac{\xi^2}{r_p^2} \right)^{-a/2} \right] \quad (1)$$

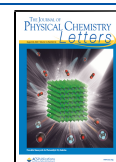
where η_0 is the viscosity of a reference buffer, A is a pre-exponential factor of the order of 1, ξ and R_H are length scales characteristic for a given system, and a is an exponent of the order of unity. R_H can be interpreted as a hydrodynamic radius of the main crowders, while ξ refers to an effective intercrowder gap, including a weak interactions factor.^{18,20} In such a fluid, small molecules ($r_p \ll \xi$) experience viscosity of the solvent, while big tracers ($r_p \gg R_H$) experience viscosity measurable by macroscopic methods. To distinguish viscosity experienced by nanoobjects, we introduce a term of nanoviscosity. We further presented applicability of this model to complex biological fluids, like cytosol of prokaryotic and eukaryotic cells,^{5,13} and we experimentally proved and applied this model for determination of oligomerization state of proteins in living cells.^{15,21}

The LSDV model relies on R_H and ξ parameters, which reflect the length scales characterizing the structure of the fluid. For the simplest case of complex fluid—a single polymer in a continuous solvent— R_H is defined as a hydrodynamic radius of polymer molecules, while ξ is mesh size or distance between intersections

Received: June 5, 2020

Accepted: July 31, 2020

Published: July 31, 2020



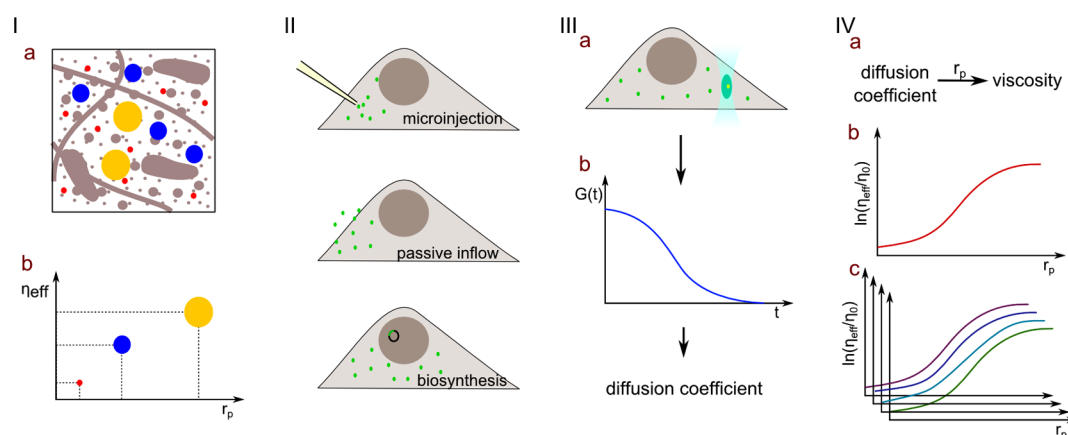


Figure 1. Principle of the research on cytoplasmic nanoviscosity. (I) Assumptions of the length-scale dependent viscosity (LSDV) model: (Ia) cytoplasm is a complex liquid containing components of various sizes. Thus, diffusion of the probes of different hydrodynamic radii (r_p) is hindered by different cytoplasmic obstacles. In the result (Ib), effective viscosity (η_{eff}) probed by tracers of different sizes increase with the size of the tracer. (II) To examine η_{eff} fluorescently labeled tracers are introduced to the cytoplasm—the mode of introduction is optimized for a given probe. (III) Next, FCS measurements are performed: (IIIa) Confocal spot is positioned in the cytoplasmic area of the cell, and fluorescence fluctuations are registered, (IIIb) autocorrelation curve (ACC) is calculated for the acquired data, and (IIIc) ACC is fitted with a proper diffusion model, and diffusion coefficient of the tracer is derived. (IV) Data collected for a set of tracers in a given cell line is used for quantitative description of the LSDV model: (IVa) η_{eff} experienced by the given probe is calculated from the diffusion coefficient, and r_p (IVb) results are plotted and fitted with eq 1; (IVc) LSDV profiles are compared between different cell lines.

of polymer chains.¹⁹ In the case of the cytoplasm, there are different types of crowders (proteins, macromolecular complexes, organelles, or cytoskeleton), and thus only effective $R_{\text{H,eff}}$ and ξ_{eff} can be derived. These parameters seemed to be unique for every cell type and culture conditions. Cells of different types differ in terms of morphology, function, or gene expression. These differences can also have an impact on nanoviscosity-like numbers, and types of metabolites and proteins would vary.

In this paper, we present a systematic, experimental study on nanoviscosity profiles of seven different cell types. The principle of this work is shown in Figure 1. Biologically inert tracers (dye molecules, fluorescent proteins, fluorescently labeled polymers, and nanoparticles) of size r_p were introduced into cells, and their diffusion coefficients were measured by fluorescence correlation spectroscopy (FCS). Many works utilize FCS or its variants in cells;^{10,22–30} however, the systematic study on the nanoviscosity at different length scales—necessary for proper data analysis—is still needed. Performance of FCS in living cells enabled reliable results achievable in mild, physiologically relevant conditions.^{14,15,31} Tracers were chosen to cover all length scales essential for cell physiology (diameters from 1 to 150 nm): metabolites, macromolecular complexes, proteins, nucleic acids, and vesicles. Cell lines were chosen to cover representatives of each group: cancerous or normal; epithelial or mesenchymal; male or female donor. Effective viscosity was measured at different length scales in every cell line, and it was confirmed that effective viscosity of cytoplasm is length-scale dependent on the majority of human cell lines.

■ LENGTH-SCALE DEPENDENT VISCOSITY OF CYTOPLASM

The LSDV model predicts that tracers of different hydrodynamic radii would experience different effective viscosity of cytoplasm, as only those obstacles which are of similar or smaller size than the tracer would have an impact on η_{eff} (Figure 1, panel I). To confirm this prediction, tracers of defined hydrodynamic radii, ranging from 0.65 to 81 nm, were introduced to cytoplasmic area of cells via microinjection (dextrans and

nanoparticles), passive inflow (Calcein-AM), or biosynthesis upon transfection (proteins) (Figure 1, panel II). We applied the core-shell type of nanoparticles to avoid the impact of nanoparticle size on FCS measurements.^{32,33} Full information on tracers used in the experiments is presented in Supporting Information 1 and 2 (SI 1, SI 2). Cells filled with tracers at final concentrations of 1–100 nM in the cytoplasm were further examined under the confocal microscope. Focal volume was positioned in the cytoplasmic area of viable cells, and FCS data was acquired (Figure 1, panel III). Each FCS experiment was preceded with careful calibration (see SI 1).^{14,34} Diffusion coefficients were derived for each type of probe (see SI 3 for details), and results were averaged for each of the cell lines considered in this study. Diffusion coefficients obtained in the cytoplasm (D) were compared to diffusion coefficients measured in water (D_0) for the same probes and temperature. Following the Stokes–Sutherland–Einstein relation, relative viscosity was calculated as follows: $\eta_{\text{eff}}/\eta_0 = D_0/D$. η_{eff}/η_0 experienced by the probe was plotted against r_p for each of the cell lines (Figure 1, panel IV).

The results obtained for six cell lines (HeLa, HepG2, MCF-7, A549, HSAEC, and U2-OS) are compiled in Figure 2. Error bars represent standard deviations reflecting the intercellular variability of the results. Possible intracellular variability was neglected, as discussed in SI 4. For each of the cell lines listed above, the effective viscosity of the cytoplasm is increasing with the size of the probing tracer. Although absolute values of η_{eff} slightly differ in particular cell lines, the trend is common in all cells of this group. The results were fitted with the LSDV model (eq 1), with following parameters: $R_{\text{H}} = 20 \pm 11$ nm, $\xi = 4.6 \pm 0.7$ nm, $a = 0.57 \pm 0.14$. a was fixed to 1.3 following our previous results.¹³ The values of the parameters of the LSDV model provide information regarding the rheological structure of the cytosol.¹⁹ Exponent $a < 1$ is characteristic for entangled polymer solutions.^{18,19} R_{H} is attributed to the size of major crowders in the complex liquid. $R_{\text{H}} = 20$ nm suggests that major crowders are of diameters ~ 40 nm, which correspond to large cytoplasmic structures, such as vesicles, mRNA molecules, or ribo-

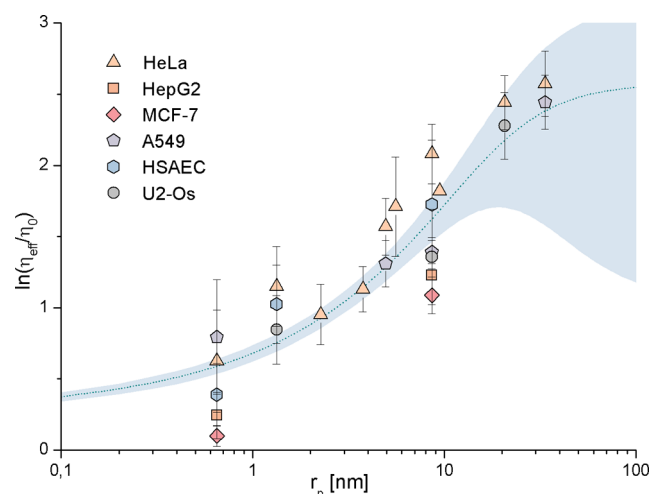


Figure 2. Nanoviscosity measured in six different cell lines. Experimental results are presented as scatter. Each point represents the average value obtained from at least 10 cells from two independent inoculations. Error bars correspond to standard deviations. Dashed line represents LSDV model (eq 1) fitted to experimental data with the following parameters: $A = 1.3$ (fixed), $R_H = 20 \pm 11$ nm, $\xi = 4.6 \pm 0.7$ nm, $a = 0.57 \pm 0.14$. Shading represents the error of the model calculated using the total differential method.

somes.^{35–37} The length-scale ξ is defined as an average radius of a mesh created by major crowders.¹⁹ $\xi \approx 4.6$ nm corresponds to the size of proteins. Thus, diffusion of proteins is affected by big crowders in the cytoplasm, while smaller metabolites experience viscosity of the solvent.

Our results, presented in Figure 2, were compared to measurements reported by other groups.^{10,13,30,38–40} The results of the comparison are shown in SI5 (Figure SI5). In general, our results are in good agreement with scattered data reported by other groups, with mismatches that could be attributed to different methods of measurements.

GEL-LIKE STRUCTURE OF CYTOPLASM

Diffusion coefficients of the probes of hydrodynamic radii smaller than 50 nm could have been measured in the cytoplasm using FCS. Larger probes, however, were more challenging: only a few autocorrelation curves were interpretable, and it was much too little for proper data analysis. We decided to support the FCS technique with its variant—Raster Image Correlation Spectroscopy (RICS).⁴¹

Fluorescent nanoparticles of diameters exceeding 100 nm were introduced via microinjection to the cytoplasm of HeLa cells and fibroblasts, and RICS analysis was performed. It turned out that no diffusion-dependent correlation could have been detected using RICS. Frame-by-frame analysis of the pictures revealed that long time and range translational diffusion could not be detected for nanoparticles of $r_p > 50$ nm (see Supplementary Movie). On the contrary, nanoparticles are trapped and oscillating in single spots. It seems like large cytoplasmic structures—like cytoskeleton or endoplasmic reticulum—create a gel-like structure of the mesh size ~ 100 nm. The size of the mesh differs in different cells or regions, as nanoparticles of $r_p = 68$ nm exhibited free diffusion (proper FCS autocorrelation curves) in several cases in HeLa cells. On the other hand, the majority of image series of nanoparticles of $r_p = 68$ or 81 nm revealed particle trapping. Our observation of a gel-

like structure filled with a liquid phase is in good correlation with previous atomic force microscopy measurements.³⁸

NANOVISCOSITY IN DIFFERENT CELLS

There is striking compliance of the nanoviscosity profiles obtained for different cell lines (Figure 3a–d). It seems that the LSDV model is universal regardless of the original tissue, type of the cell, gender, or age of the donor. Although values of nanoviscosity for given length scales can slightly differ between different cells, the overall trend is similar—the nanoviscosity is length-scale dependent. The majority of batteries used in the study exhibit cytoplasmic viscosity of approximately 2 viscosities of water for probes of $r_p < 1$ nm, while for probes of $r_p > 20$ nm the nanoviscosity reaches the value of approximately 10 viscosities of water. We assumed four factors that could impact nanometabolism via nanoviscosity of the cytoplasm: tissue type (epithelial or mesenchymal), disease (cancerous or non-cancerous), gender of the donor (male or female), and age of the donor (young or adult); see SI 6. No differences could have been spotted between the cell groups in any of the four categories. Additionally, for our further work, we profiled nanoviscosity of other cell lines (primary mammary epithelium and triple-negative breast cancer cells; data not shown), and their nanoviscosity is comparable with the values presented in Figure 2. Stability of the cytoplasmic nanoviscosity is particularly surprising for the case of cancer and healthy cells, which are reported to differ in terms of microscopic rheological parameters.^{42,43}

The presented results show that nanoviscosity is somehow conserved in human cells, apart from the viscosity of the cytoplasmic matrix of small molecules ($r_p < 1$ nm); the LSDV profiles—depending on the abundance of organelles and macromolecules—are also the same. This stability is a surprising result, in terms of widely reported variability in cell sizes,⁴⁴ as well as protein expression levels.⁴⁵ In our previous work,³¹ we presented that nanoviscosity sensed by EGFP ($r_p = 2.3$ nm) is also constant (with a slight, 30% increase during S phase) during the whole cell cycle of HeLa cells. These results, together with those presented in the present work, provide a picture of stable nanoviscosity in human cells. Future questions arise from these observations: whether nanoviscosity has a biological impact and is conserved on a level optimal for cell homeostasis.

FIBROBLASTS EXHIBIT DIFFERENT NANOVISCOSITY THAN OTHER CELLS

Primary skin fibroblasts are the only cells for which nanoviscosity profile is not length-scale dependent in the range of length scales of $1 \text{ nm} < r_p < 20 \text{ nm}$. Thus, the nanoviscosity profile of fibroblasts deviates from the results for all other cell lines (Figure 3: e). It is a surprising result, as other mesenchymal (Figure 3: a) or noncancerous (Figure 3: b) cells exhibited “usual” LSDV profiles. On the other hand, cytoplasmic viscosities were similar in fibroblasts and other cells for the probes larger than 20 nm. The nanoviscosity for smaller probes in the cytoplasm of fibroblasts was independent of the passage number (see SI 7).

To investigate a potential source of differences in nanoviscosity, we imaged large cytoplasmic obstacles (cytoskeleton: actin and tubulin, and endoplasmic reticulum, ER) in fibroblasts, HeLa, A549, and U2-Os cells (Figure 4). Fibroblasts were imaged as cells of interest, according to their extraordinary nanoviscosity. HeLa and A549 were chosen as control cancer

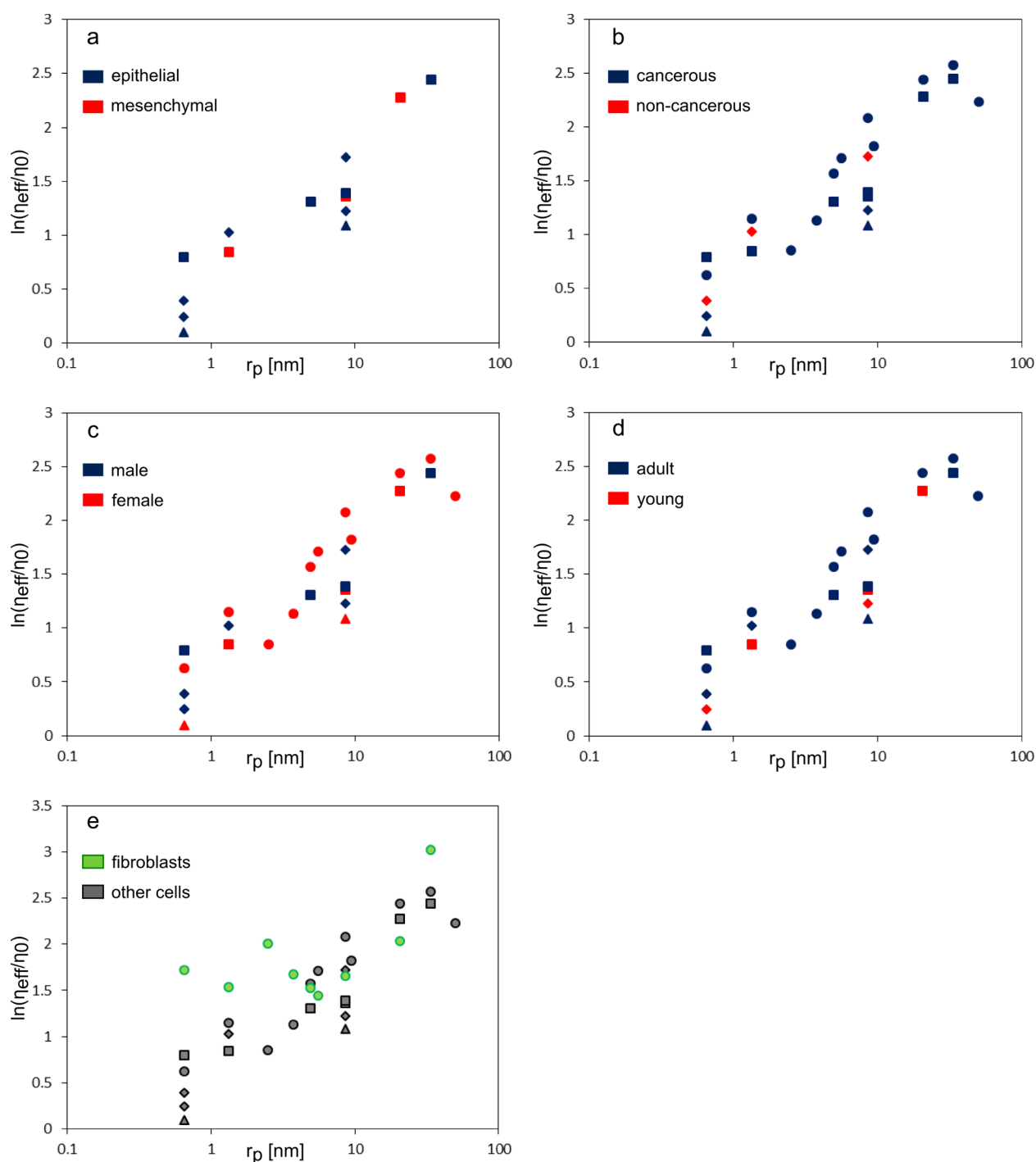


Figure 3. Comparison of nanoviscosity in different cell types. Graphs represent average relative nanoviscosity measured in the cytoplasm of different cells and plotted against hydrodynamic radii of the tracers probing the viscosity (data consistent with Figure 2) (a–d) Cell lines used in the study were divided into groups (see SI 5), according to (a) tissue origin, (b) disease, (c) gender of donor, or (d) age of donor. No deviations of the viscosity could have been observed between these groups. (e) Fibroblasts were the only cell line in which nanoviscosity was found to differ from the major trend for small probes ($r_p < 10$ nm).

epithelial cells, while U2-OS were selected as control cancer mesenchymal cells. In the first experiment (Figure 4: a), actin and tubulin were stained using ligands specific for these proteins (phalloidin-based and paclitaxel-based, respectively). At least ten cells were imaged for every cell type. No distinct differences in cytoskeleton abundances were observed. The second experiment (Figure 4: b) included the immunostaining of ER. Again, at least ten cells were imaged for every cell type. In this

variant, it was observed that the ER is much more abundant in fibroblasts than other cells. The abundance of the stained ER was quantified (see SI 8), and results are presented in Figure 5. We decided to take into account the total size of the ER, rather than the signal intensity, which may vary from cell to cell according to different protein expression levels.⁴⁶ A significant difference in ER abundance was observed between fibroblasts and other cells: ER covered an average of 67% of the cytoplasmic

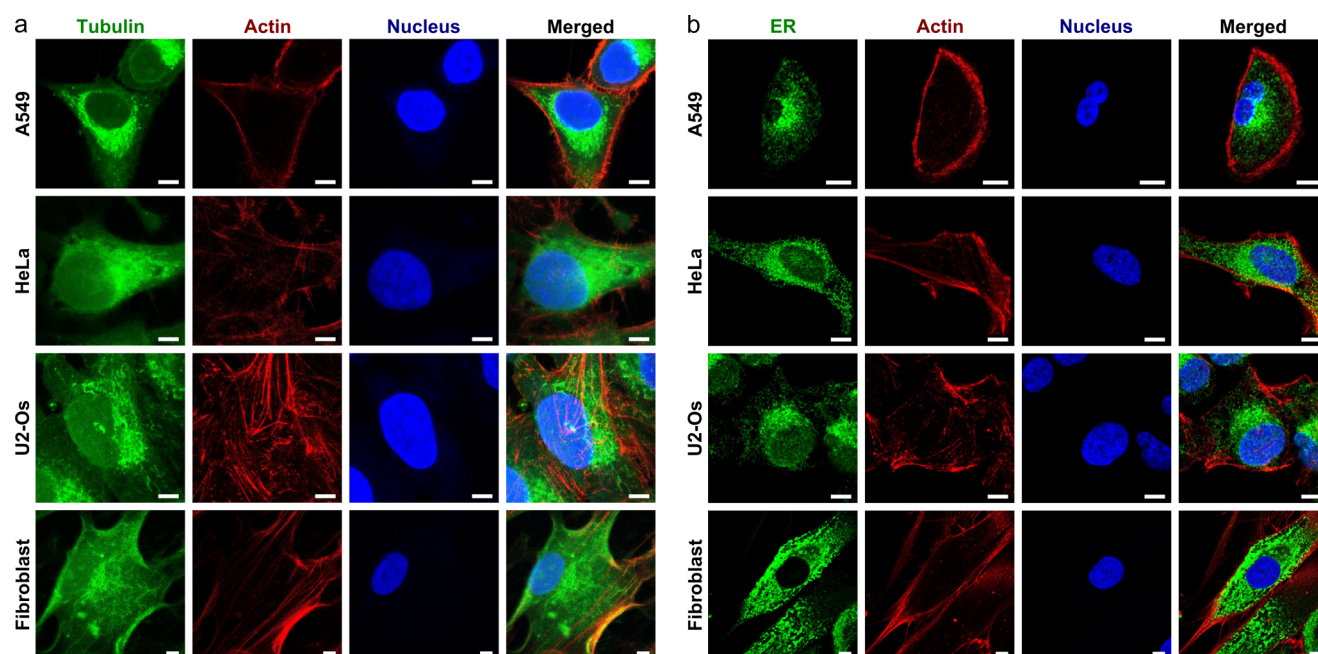


Figure 4. Confocal images of subcellular structures of four cell lines: A549, HeLa, U2-Os, and Fibroblasts. (a) Staining of cytoskeletal proteins (actin and tubulin) showed no particular differences between cell types. (b) Immunostaining of endoplasmic reticulum (ER) revealed a high abundance of ER in fibroblasts comparing to three other cell lines. Scale bars correspond to 10 μm .

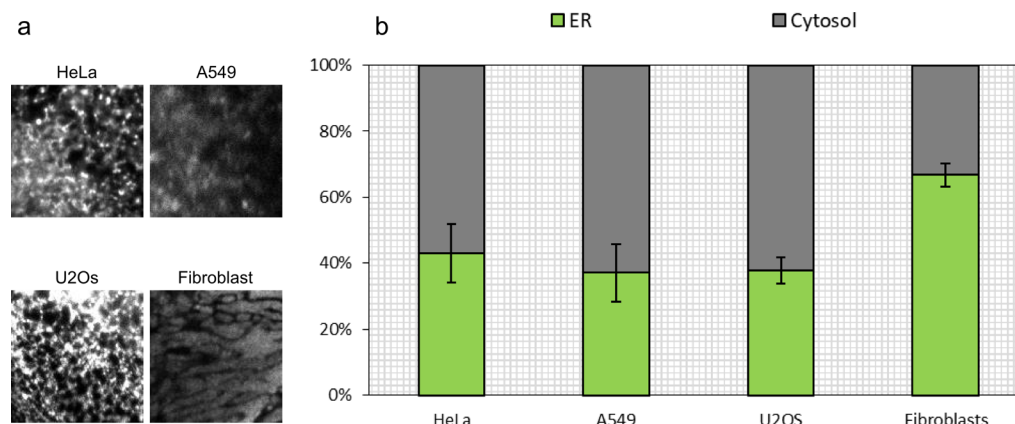


Figure 5. Quantification of ER abundance in different cell types. (a) Example confocal images of ER in different cells. (b) Average abundance of ER (white pixels) and cytosol (black pixels) in cells of various types.

area in fibroblasts, while in A549, HeLa, and U2-Os, it was 37%, 43%, and 38%, respectively. As a complement, the cytosol (liquid phase of cytoplasm) of the fibroblasts was compressed into 33% of the cytoplasmic volume, while in other cells, it is an average of 61%.

From the diffusion point of view, the endoplasmic reticulum is a set of membrane walls crossing the medium. Its presence is included in the η_{eff} measured in our FCS experiments. The focal volume has a cross section of diameter ~ 400 nm, which can consist of ER cisterna or other membrane obstacles (such as mitochondria, lysosomes, etc.). With the higher ER or organelle abundance, the number of membrane walls increases. There is a known phenomenon of near-wall diffusion hindrance,⁴⁷ causing an increase of effective viscosity. Also, our previous studies on lamellar phases revealed an increase of continuous phase viscosity, comparing to the same solvent with no lamella.⁴⁸ These observations are consistent with our measurements in fibroblasts—more abundant ER can possibly cause matrix

viscosity increase. This effect is less pronounced for bigger length scales—for tracers of $r_p > 20$ nm, cytoplasmic viscosities of fibroblasts reach values similar to every other cell line examined in this study.

To conclude, we performed a systematic study on cytoplasmic nanostructure in seven different cell types. Cell lines used in this study represented different origins (epithelial or mesenchymal, cancer or healthy, male or female, young or adult). We probed cytoplasmic nanoviscosity at length scales in the range of 1–150 nm, revealing length-scale dependent viscosity profiles present in the majority of cells. We provided the model equation describing nanoviscosity, and derived length scales characteristic for the cytoplasm. It was shown that mRNA, ribosomes, and vesicles are major cytoplasmic crowders. It was also demonstrated that nanoparticles of diameters bigger than 100 nm are unable to diffuse freely through the cytoplasm, suggesting a critical length scale crossover to gel-like structure in the cytoplasm.

The cytoplasmic nanoviscosity is conserved in the majority of human cell lines. The only cells differing from the major trend are fibroblasts. The potential source of this discrepancy can be the abundance of intracellular membrane structures, which we identified at the example of the endoplasmic reticulum. Though, the length-scale dependent viscosity model seems to be universal for human cells, regardless of age, disease, or type of tissue. Moreover, in our previous work,³¹ we presented the stability of cytoplasmic viscosity for the whole cell cycle. All these results indicate that nanoviscosity can play a vital role in cellular homeostasis maintenance, and some unknown mechanism keeps it stable in single cells and between cell types. These observations open a new field of questions about the role and regulation of the physical properties of cells.

■ ASSOCIATED CONTENT

Supporting Information

The Supporting Information is available free of charge at <https://pubs.acs.org/doi/10.1021/acs.jpclett.0c01748>.

Materials and methods; Characteristics of fluorescent tracers; Autocorrelation curve fitting; Variability of nanoviscosity: intracellular vs intercellular; Comparison of cytoplasmic viscosity reported in different studies; Types of cells used in experiments; Effect of passage number on the viscosity of fibroblasts; Quantification of ER abundance (PDF)

Supplementary movie: Raster Image Correlation Spectroscopy (MOV)

■ AUTHOR INFORMATION

Corresponding Authors

Karina Kwapiszewska – Institute of Physical Chemistry, Polish Academy of Sciences, Warsaw 01-224, Poland;
Email: kkwapiszewska@ichf.edu.pl

Robert Holyst – Institute of Physical Chemistry, Polish Academy of Sciences, Warsaw 01-224, Poland; orcid.org/0000-0002-3211-4286; Email: rholyt@ichf.edu.pl

Authors

Krzysztof Szczepański – Institute of Physical Chemistry, Polish Academy of Sciences, Warsaw 01-224, Poland

Tomasz Kalwarczyk – Institute of Physical Chemistry, Polish Academy of Sciences, Warsaw 01-224, Poland

Bernadeta Michalska – Nencki Institute of Experimental Biology, Warsaw 02-093, Poland

Paulina Patalas-Krawczyk – Nencki Institute of Experimental Biology, Warsaw 02-093, Poland

Jędrzej Szymański – Nencki Institute of Experimental Biology, Warsaw 02-093, Poland

Tomasz Andryszewski – Institute of Physical Chemistry, Polish Academy of Sciences, Warsaw 01-224, Poland

Michalina Iwan – Institute of Physical Chemistry, Polish Academy of Sciences, Warsaw 01-224, Poland

Jerzy Duszyński – Nencki Institute of Experimental Biology, Warsaw 02-093, Poland

Complete contact information is available at:

<https://pubs.acs.org/doi/10.1021/acs.jpclett.0c01748>

Notes

The authors declare no competing financial interest.

■ ACKNOWLEDGMENTS

The authors would like to acknowledge Dr. Krzysztof Sozański for his help with RICS experiments. This work was supported by the Maestro grant UMO-2016/22/A/ST4/00017 from the National Science Centre, Poland.

■ REFERENCES

- (1) Feist, A. M.; Herrgård, M. J.; Thiele, I.; Reed, J. L.; Palsson, B. Ø. Reconstruction of Biochemical Networks in Microorganisms. *Nat. Rev. Microbiol.* **2009**, *7* (2), 129–143.
- (2) Meléndez-Hevia, E.; Waddell, T. G.; Cascante, M. The Puzzle of the Krebs Citric Acid Cycle: Assembling the Pieces of Chemically Feasible Reactions, and Opportunism in the Design of Metabolic Pathways during Evolution. *J. Mol. Evol.* **1996**, *43* (3), 293–303.
- (3) Ohtsubo, K.; Marth, J. D. Glycosylation in Cellular Mechanisms of Health and Disease. *Cell* **2006**, *126* (5), 855–867.
- (4) Tappy, L.; Le, K.-A. Metabolic Effects of Fructose and the Worldwide Increase in Obesity. *Physiol. Rev.* **2010**, *90* (1), 23–46.
- (5) Tabaka, M.; Kalwarczyk, T.; Szymanski, J.; Hou, S.; Holyst, R. The Effect of Macromolecular Crowding on Mobility of Biomolecules, Association Kinetics, and Gene Expression in Living Cells. *Front. Phys.* **2014**, *2* (54), 1–14.
- (6) Dill, K. A.; Ghosh, K.; Schmit, J. D. Physical Limits of Cells and Proteomes. *Proc. Natl. Acad. Sci. U. S. A.* **2011**, *108* (44), 17876–17882.
- (7) Tanaka, A.; Fukuoka, Y.; Morimoto, Y.; Honjo, T.; Koda, D.; Goto, M.; Maruyama, T. Cancer Cell Death Induced by the Intracellular Self-Assembly of an Enzyme-Responsive Supramolecular Gelator. *J. Am. Chem. Soc.* **2015**, *137* (2), 770–775.
- (8) Einstein, A. Über Die von Der Molekularkinetischen Theorie Der Wärme Geforderte Bewegung von in Ruhenden Flüssigkeiten Suspendierten Teilchen. *Ann. Phys.* **1905**, *322*, 549–560.
- (9) Sutherland, W. LXXXV. A Dynamical Theory of Diffusion for Non-Electrolytes and the Molecular Mass of Albumin. *London, Edinburgh, Dublin Philos. Mag. J. Sci.* **1905**, *9* (54), 781–785.
- (10) Baum, M.; Erdel, F.; Wachsmuth, M.; Rippe, K. Retrieving the Intracellular Topology from Multi-Scale Protein Mobility Mapping in Living Cells. *Nat. Commun.* **2014**, *5*, 1–12.
- (11) Ruan, Q.; Chen, Y.; Gratton, E.; Glaser, M.; Mantulin, W. W. Cellular Characterization of Adenylate Kinase and Its Isoform: Two-Photon Excitation Fluorescence Imaging and Fluorescence Correlation Spectroscopy. *Biophys. J.* **2002**, *83* (6), 3177–3187.
- (12) Parker, W. C.; Chakraborty, N.; Vrikkis, R.; Elliott, G.; Smith, S.; Moyer, P. J. High-Resolution Intracellular Viscosity Measurement Using Time-Dependent Fluorescence Anisotropy. *Opt. Express* **2010**, *18* (16), 16607.
- (13) Kalwarczyk, T.; Ziębac, N.; Bielejewska, A.; Zaboklicka, E.; Koynov, K.; Szymański, J.; Wilk, A.; Patkowski, A.; Gapiński, J.; Butt, H.-J.; Holyst, R. Comparative Analysis of Viscosity of Complex Liquids and Cytoplasm of Mammalian Cell at the Nanoscale. *Nano Lett.* **2011**, *11*, 2157–2163.
- (14) Kalwarczyk, T.; Kwapiszewska, K.; Szczepański, K.; Sozański, K.; Szymanski, J.; Michalska, B.; Patalas-Krawczyk, P.; Duszyński, J.; Holyst, R. Apparent Anomalous Diffusion in the Cytoplasm of Human Cells: The Effect of Probes' Polydispersity. *J. Phys. Chem. B* **2017**, *121* (42), 9831–9837.
- (15) Kwapiszewska, K.; Kalwarczyk, T.; Michalska, B.; Szczepański, K.; Szymański, J.; Patalas-Krawczyk, P.; Andryszewski, T.; Iwan, M.; Duszyński, J.; Holyst, R. Determination of Oligomerization State of Drp1 Protein in Living Cells at Nanomolar Concentrations. *Sci. Rep.* **2019**, *9* (1), 5906.
- (16) Holyst, R.; Bielejewska, A.; Szymański, J.; Wilk, A.; Patkowski, A.; Gapiński, J.; Zywociński, A.; Kalwarczyk, T.; Kalwarczyk, E.; Tabaka, M.; Zibacz, N.; Wieczorek, S. A Scaling Form of Viscosity at All Length-Scales in Poly(Ethylene Glycol) Solutions Studied by Fluorescence Correlation Spectroscopy and Capillary Electrophoresis. *Phys. Chem. Chem. Phys.* **2009**, *11* (40), 9025–9032.
- (17) Sozański, K.; Wiśniewska, A.; Kalwarczyk, T.; Holyst, R. Activation Energy for Mobility of Dyes and Proteins in Polymer

Solutions: From Diffusion of Single Particles to Macroscale Flow. *Phys. Rev. Lett.* **2013**, *111* (22), 1–5.

(18) Wiśniewska, A.; Sozański, K.; Kalwarczyk, T.; Kędra-Królik, K.; Pieper, C.; Wiczorek, S. A.; Jakiela, S.; Enderlein, J.; Holyst, R. Scaling of Activation Energy for Macroscopic Flow in Poly(Ethylene Glycol) Solutions: Entangled - Non-Entangled Crossover. *Polymer* **2014**, *55* (18), 4651–4657.

(19) Kalwarczyk, T.; Sozanski, K.; Ochab-Marcinek, A.; Szymanski, J.; Tabaka, M.; Hou, S.; Holyst, R. Motion of Nanoprobes in Complex Liquids within the Framework of the Length-Scale Dependent Viscosity Model. *Adv. Colloid Interface Sci.* **2015**, *223*, 55–63.

(20) Kalwarczyk, T.; Tabaka, M.; Holyst, R. Biologistics-Diffusion Coefficients for Complete Proteome of Escherichia Coli. *Bioinformatics* **2012**, *28* (22), 2971–2978.

(21) Michalska, B. M.; Kwapiszewska, K.; Szczepanowska, J.; Kalwarczyk, T.; Patalas-Krawczyk, P.; Szczepański, K.; Holyst, R.; Duszyński, J.; Szymański, J. Insight into the Fission Mechanism by Quantitative Characterization of Drp1 Protein Distribution in the Living Cell. *Sci. Rep.* **2018**, *8* (1), 8122.

(22) Chen, J.; Irudayaraj, J. Fluorescence Lifetime Cross Correlation Spectroscopy Resolves EGFR and Antagonist Interaction in Live Cells. *Anal. Chem.* **2010**, *82* (15), 6415–6421.

(23) Schwille, P.; Haupts, U.; Maiti, S.; Webb, W. W. Molecular Dynamics in Living Cells Observed by Fluorescence Correlation Spectroscopy with One- and Two-Photon Excitation. *Biophys. J.* **1999**, *77* (4), 2251–2265.

(24) Du, Z.; Dong, C.; Ren, J. A Study of the Dynamics of PTEN Proteins in Living Cells Using in Vivo Fluorescence Correlation Spectroscopy. *Methods Appl. Fluoresc.* **2017**, *5* (2), 024008.

(25) Oura, M.; Yamamoto, J.; Ishikawa, H.; Mikuni, S.; Fukushima, R.; Kinjo, M. Polarization-Dependent Fluorescence Correlation Spectroscopy for Studying Structural Properties of Proteins in Living Cell. *Sci. Rep.* **2016**, *6* (31091), 1–7.

(26) Guan, Y.; Meurer, M.; Raghavan, S.; Rebane, A.; Lindquist, J. R.; Santos, S.; Kats, I.; Davidson, M. W.; Mazitschek, R.; Hughes, T. E.; Drobizhev, M.; Knop, M.; Shah, J. V. Live-Cell Multiphoton Fluorescence Correlation Spectroscopy with an Improved Large Stokes Shift Fluorescent Protein. *Mol. Biol. Cell* **2015**, *26* (11), 2054–2066.

(27) Broderick, R.; Ramadurai, S.; Tóth, K.; Togashi, D. M.; Ryder, A. G.; Langowski, J.; Nasheuer, H. P. Cell Cycle-Dependent Mobility of Cdc45 Determined in Vivo by Fluorescence Correlation Spectroscopy. *PLoS One* **2012**, *7* (4), No. e35537.

(28) Rezgui, R.; Blumer, K.; Yeoh-Tan, G.; Trexler, A. J.; Magzoub, M. Precise Quantification of Cellular Uptake of Cell-Penetrating Peptides Using Fluorescence-Activated Cell Sorting and Fluorescence Correlation Spectroscopy. *Biochim. Biophys. Acta, Biomembr.* **2016**, *1858* (7), 1499–1506.

(29) Anton, H.; Taha, N.; Boutant, E.; Richert, L.; Khatter, H.; Klaholz, B.; Rondé, P.; Réal, E.; De Rocquigny, H.; Mély, Y. Investigating the Cellular Distribution and Interactions of HIV-1 Nucleocapsid Protein by Quantitative Fluorescence Microscopy. *PLoS One* **2015**, *10* (2), No. e0116921.

(30) Xiang, L.; Chen, K.; Yan, R.; Li, W.; Xu, K. Single-Molecule Displacement Mapping Unveils Nanoscale Heterogeneities in Intracellular Diffusivity. *Nat. Methods* **2020**, *17*, 524–530.

(31) Szczepański, K.; Kwapiszewska, K.; Holyst, R. Stability of Cytoplasmic Nanoviscosity during Cell Cycle of HeLa Cells Synchronized with Aphidicolin. *Sci. Rep.* **2019**, *9*, 16486.

(32) Deptuła, T.; Buitenhuis, J.; Jarzębski, M.; Patkowski, A.; Gapinski, J. Size of Submicrometer Particles Measured by FCS: Correction of the Confocal Volume. *Langmuir* **2015**, *31*, 6681–6687.

(33) Gapinski, J.; Jarzębski, M.; Buitenhuis, J.; Deptuła, T.; Mazuryk, J.; Patkowski, A. Structure and Dimensions of Core-Shell Nanoparticles Comparable to the Confocal Volume Studied by Means of Fluorescence Correlation Spectroscopy. *Langmuir* **2016**, *32*, 2482–2491.

(34) Banachowicz, E.; Patkowski, A.; Meier, G.; Klamecka, K.; Gapiński, J. Successful FCS Experiment in Nonstandard Conditions. *Langmuir* **2014**, *30* (29), 8945–8955.

(35) Freitas, R. A.; Merkle, R. C. *Kinematic Self-Replicating Machines*; Landes Bioscience/Eurekah.com, 2004.

(36) Gopal, A.; Zhou, Z. H.; Knobler, C. M.; Gelbart, W. M. Visualizing Large RNA Molecules in Solution. *RNA* **2012**, *18* (2), 284–299.

(37) Takamori, S.; Holt, M.; Stenius, K.; Lemke, E. A.; Grønborg, M.; Riedel, D.; Urlaub, H.; Schenck, S.; Brügger, B.; Ringler, P.; Müller, S. A.; Rammner, B.; Gräter, F.; Hub, J. S.; De Groot, B. L.; Mieskes, G.; Moriyama, Y.; Klingauf, J.; Grubmüller, H.; Heuser, J.; Wieland, F.; Jahn, R. Molecular Anatomy of a Trafficking Organelle. *Cell* **2006**, *127* (4), 831–846.

(38) Moeendarbary, E.; Valon, L.; Fritzsche, M.; Harris, A. R.; Moulding, D. A.; Thrasher, A. J.; Stride, E.; Mahadevan, L.; Charras, G. T. The Cytoplasm of Living Cells Behaves as a Poroelastic Material. *Nat. Mater.* **2013**, *12* (3), 253–261.

(39) Nakane, Y.; Sasaki, A.; Kinjo, M.; Jin, T. Bovine Serum Albumin-Coated Quantum Dots as a Cytoplasmic Viscosity Probe in a Single Living Cell. *Anal. Methods* **2012**, *4* (7), 1903–1905.

(40) Daddysman, M. K.; Fecko, C. J. Revisiting Point FRAP to Quantitatively Characterize Anomalous Diffusion in Live Cells. *J. Phys. Chem. B* **2013**, *117* (5), 1241–1251.

(41) Rossow, M. J.; Sasaki, J. M.; Digman, M. A.; Gratton, E. Raster Image Correlation Spectroscopy in Live Cells. *Nat. Protoc.* **2010**, *5*, 1761.

(42) Wang, K.; Sun, X. H.; Zhang, Y.; Zhang, T.; Zheng, Y.; Wei, Y. C.; Zhao, P.; Chen, D. Y.; Wu, H. A.; Wang, W. H.; Long, R.; Wang, J. B.; Chen, J. Characterization of Cytoplasmic Viscosity of Hundreds of Single Tumour Cells Based on Micropipette Aspiration. *R. Soc. Open Sci.* **2019**, *6*, 181707.

(43) Lekka, M. Discrimination Between Normal and Cancerous Cells Using AFM. *Bionanoscience* **2016**, *6* (1), 65–80.

(44) Moran, U.; Phillips, R.; Milo, R. SnapShot: Key Numbers in Biology. *Cell* **2010**, *141* (7), 1262.

(45) Geiger, T.; Wehner, A.; Schaab, C.; Cox, J.; Mann, M. Comparative Proteomic Analysis of Eleven Common Cell Lines Reveals Ubiquitous but Varying Expression of Most Proteins. *Mol. Cell. Proteomics* **2012**, *11* (3), M111.014050.

(46) Thul, P. J.; Akesson, L.; Wiking, M.; Mahdessian, D.; Geladaki, A.; Ait Blal, H.; Alm, T.; Asplund, A.; Björk, L.; Breckels, L. M.; Bäckström, A.; Danielsson, F.; Fagerberg, L.; Fall, J.; Gatto, L.; Gnann, C.; Hober, S.; Hjelmare, M.; Johansson, F.; Lee, S.; Lindskog, C.; Mulder, J.; Mulvey, C. M.; Nilsson, P.; Oksvold, P.; Rockberg, J.; Schutten, R.; Schwenk, J. M.; Sivertsson, A.; Sjöstedt, E.; Skogs, M.; Stadler, C.; Sullivan, D. P.; Tegel, H.; Winsnes, C.; Zhang, C.; Zwahlen, M.; Mardinoglu, A.; Pontén, F.; Von Feilitzen, K.; Lilley, K. S.; Uhlén, M.; Lundberg, E. A Subcellular Map of the Human Proteome. *Science (Washington, DC, U. S.)* **2017**, *356* (6340), No. eaal3321.

(47) Choi, C. K.; Margraves, C. H.; Kihm, K. D. Examination of Near-Wall Hindered Brownian Diffusion of Nanoparticles: Experimental Comparison to Theories by Brenner (1961) and Goldman et Al. (1967). *Phys. Fluids* **2007**, *19*, 103305.

(48) Szymański, J.; Wilk, A.; Holyst, R.; Roberts, G.; Sinclair, K.; Kowalski, A. Micro- and Macro-Shear Viscosity in Dispersed Lamellar Phases. *J. Non-Newtonian Fluid Mech.* **2008**, *148* (1–3), 134–140.